# Fast, High Resolution, and Wide Modulus Range Nanomechanical Mapping with Bimodal Tapping Mode

Marta Kocun, Aleksander Labuda, Waiman Meinhold, Irène Revenko, and Roger Proksch*[ID]

Asylum Research—An Oxford Instruments Company, Santa Barbara, California 93117, United States

Ⓢ *Supporting Information*

ABSTRACT: Tapping mode atomic force microscopy (AFM), also known as amplitude modulated (AM) or AC mode, is a proven, reliable, and gentle imaging mode with widespread applications. Over the several decades that tapping mode has been in use, quantification of tip–sample mechanical properties such as stiffness has remained elusive. Bimodal tapping mode keeps the advantages of single-frequency tapping mode while extending the technique by driving and measuring an additional resonant mode of the cantilever. The simultaneously measured observables of this additional resonance provide the additional information necessary to extract quantitative nanomechanical information about the tip–sample mechanics. Specifically, driving the higher cantilever resonance in a frequency modulated (FM) mode allows direct measurement of the tip–sample interaction stiffness and, with appropriate modeling, the set point-independent local elastic modulus. Here we discuss the advantages of bimodal tapping, coined AM-FM imaging, for modulus mapping. Results are presented for samples over a wide modulus range, from a compliant gel (∼100 MPa) to stiff materials (∼100 GPa), with the same type of cantilever. We also show high-resolution (subnanometer) stiffness mapping of individual molecules in semicrystalline polymers and of DNA in fluid. Combined with the ability to remain quantitative even at line scan rates of nearly 40 Hz, the results demonstrate the versatility of AM-FM imaging for nanomechanical characterization in a wide range of applications.
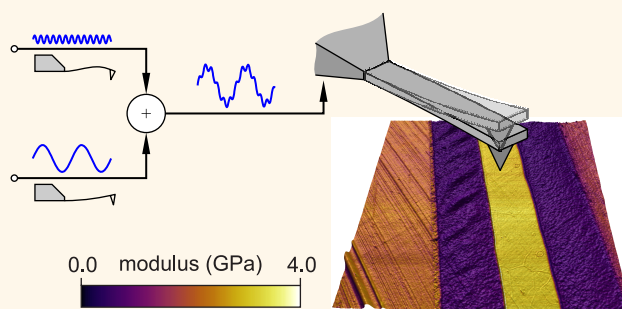
KEYWORDS: atomic force microscopy, bimodal AFM, modulus mapping, nanomechanical properties, tapping mode

T he function and performance of many emerging materials and devices depend on their nanoscale morphology, composition, and mechanical properties. However, as the length scales of these materials and devices decrease, quantitative measurements of parameters such as the elastic modulus become increasingly challenging. Thus, a nanomechanical mapping technique—an imaging technique that provides high spatial resolution simultaneously with quantitative mechanical properties—has been a long-standing goal for many fields. Atomic force microscopy (AFM) is well suited for nanoscale characterization of surfaces and interfaces, with image sizes that can range from tens of micrometers down to fractions of a nanometer. Additionally, the nondestructive nature of AFM, together with its minimal sample preparation requirements, makes it exceptionally versatile.

One of the most common measurement modes in AFM is the dynamic mode called amplitude modulation (AM-AFM), also known as tapping mode or AC mode. During AM-AFM imaging, the cantilever is excited dynamically near a resonant frequency, and the amplitude and phase of the cantilever oscillation are measured. The amplitude is used as a feedback signal for controlling the tip–sample distance in order to track sample topography. Advantages of AM-AFM include minimal tip and sample damage (which allows imaging of softer samples compared to contact mode and force mapping modes), low lateral forces, and high-resolution and very fast imaging capabilities.[1,2] A significant drawback of AM-AFM, which drives the cantilever at a single frequency, is its difficulty in quantifying sample mechanical properties. AM-AFM can only provide the ratio of storage to loss modulus, because the phase response is affected by both conservative and dissipative interactions.[3−6]

Roughly a decade ago, it was recognized that simultaneously exciting higher resonance(s) of the cantilever provides additional information regarding the tip–sample interactions.[7−11] One variation of this approach is called bimodal imaging, where two resonant modes are excited simultaneously.
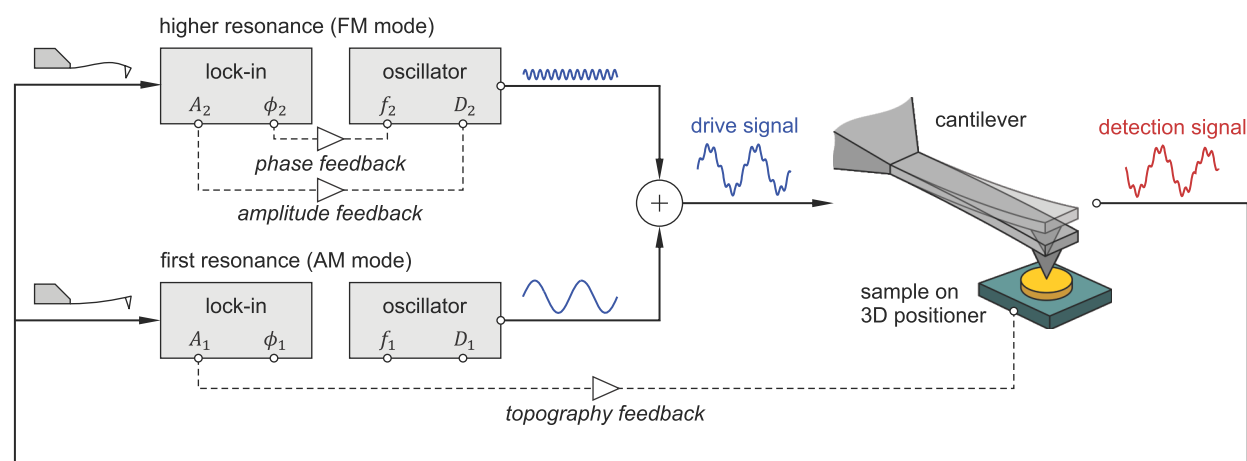
Figure 1. System diagram for bimodal AM-FM imaging mode. The first resonance of the cantilever is driven with a large amplitude A_1, and a higher resonance is driven simultaneously with a small amplitude A_2. The topography feedback loop uses the A_1 to track topography. The amplitude feedback loop maintains constant oscillation amplitude of the higher resonance. The phase feedback loop tracks the frequency of the higher resonance to drive it on resonance despite changes in sample modulus.
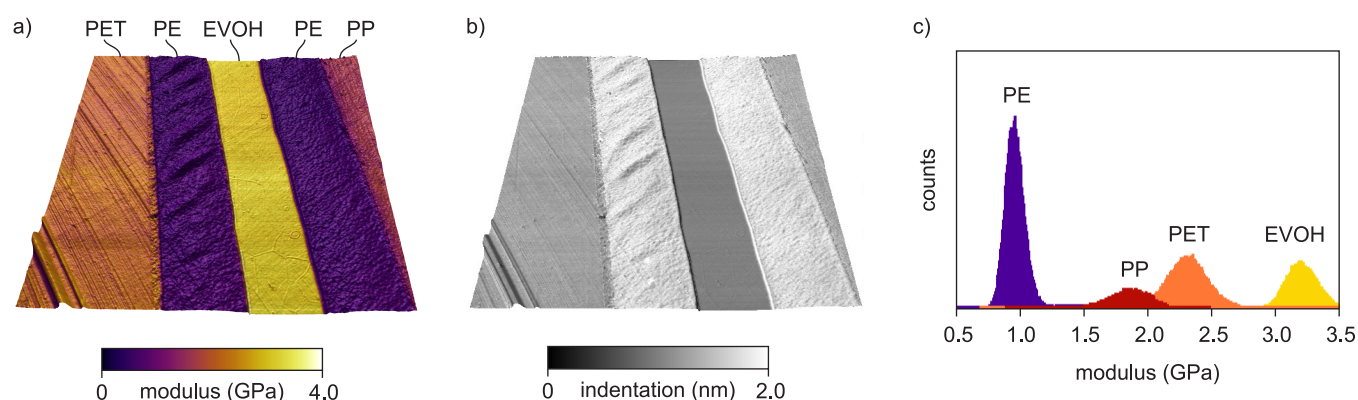

Figure 2. Maps of (a) modulus and (b) indentation depth overlaid on topography for a multilayer polymer film. (c) Histogram of the modulus map differentiates the four polymers (PE, PP, PET, EVOH) composing the multilayer film. Calibration of the tip size was performed on a polystyrene reference sample. Cantilever: Olympus AC160 with $k_1 \approx 34$ N/m, $f_1 \approx 293$ kHz, $k_2 \approx 597$ N/m, and $f_2 \approx 1.63$ MHz. Scan size 25 μm.

Bimodal AFM can be performed in different modes of operation, such as amplitude modulation (AM),[12−16] phase modulation (PM),[17−20] and frequency modulation (FM).[21−25] Originally bimodal experiments were performed in the AM-AM configuration,[8] while the FM-FM configuration was later explored by Heruzzo et al.[2]

Here, we demonstrate the capabilities of a hybrid bimodal technique for nanomechanical mapping that combines the robust simplicity of AM operation for the first resonance of the cantilever with the high sensitivity and signal-to-noise ratio of FM operation for the second resonance. This "AM-FM" imaging mode allows for a large dynamic range of measurable modulus, molecular-level spatial resolution at very fast scan speeds and quantitative mapping of moduli, stiffness and indentation depths.

RESULTS AND DISCUSSION

Bimodal AM-FM Imaging. The principles of AM-FM operation are described in Figure 1. Prior to tip−sample interaction, the first cantilever eigenmode is excited near its resonant frequency f_1 with a large amplitude (typically, $A_{1,\text{free}} \approx$ 100 nm), and the second (or higher) eigenmode is excited near its resonant frequency f_2 with a much smaller amplitude

(typically, $A_{2,\text{free}} \approx$ 1 nm). In the experiments described here, the driving force was provided by modulating the power of a blue laser focused on the base of the cantilever. The spring constants k_1 and k_2 and quality factors Q_1 and Q_2 of the first and second eigenmodes, respectively, are determined before the experiment by fitting the thermal response of the cantilever away from the surface.

Upon approaching the sample, the deflection signal of the interacting cantilever is analyzed by a lock-in amplifier to determine the amplitude A_1 and phase ϕ_1 response of the first eigenmode. The topography feedback adjusts the sample height to maintain a constant, predetermined amplitude set point $A_{1,\text{set}}$. This type of feedback is identical to that used in AM-AFM imaging for topography tracking.

The deflection signal is also analyzed by a second lock-in at the frequency of the higher eigenmode. Here, a frequency feedback loop continuously adjusts the excitation frequency by a small amount Δf_2 to maintain the second eigenmode on resonance as the tip interacts with the sample. In addition, an amplitude feedback loop is used to maintain constant oscillation amplitude of the second eigenmode. This ensures that the small amplitude of the second mode remains above the detection noise floor while remaining small relative to the
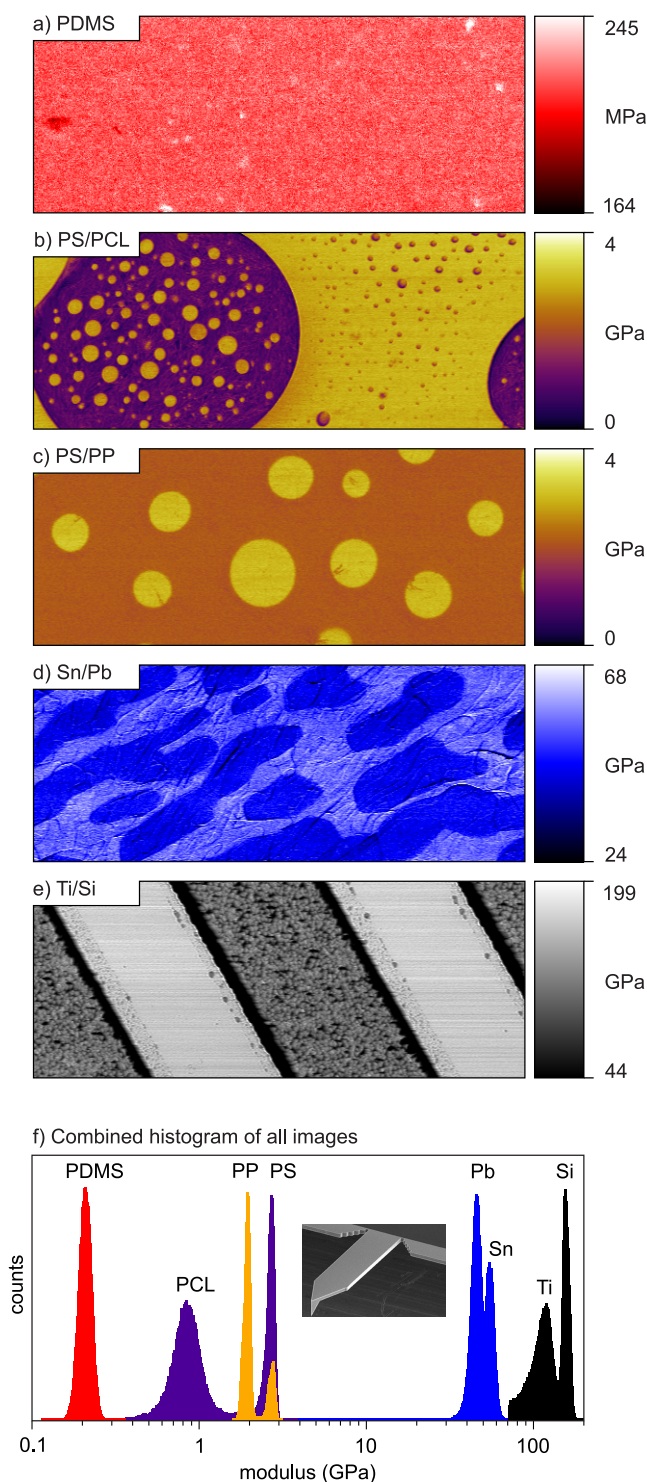
Figure 3. AM-FM modulus maps on samples with a wide range of modulus (in order of increasing modulus): (a) PDMS, (b) PS/PCL polymer blend, (c) PS/PP polymer blend, (d) Sn/Pb solder alloy, and (e) Ti thin-film stripes on Si. All images are ∼8 μm wide. (f) Combined color-coded histogram of the images in (a−e) on a logarithmic scale. The inset shows a scanning electron micrograph of an Olympus AC160 cantilever such as used in all these measurements (160 μm long, nominal $k_1 \approx 30$ N/m).

The AM-FM signals produced by this imaging feedback scheme can be used[26] to extract the maximum indentation depth δ

$$\delta = \frac{3}{4}\left(\frac{k_1}{Q_1}A_{1,\text{free}}\cos\phi_1\right)\left(\frac{2k_2\Delta f_2}{f_2}\right)^{-1} \tag{1}$$

and the effective storage modulus of the interaction E_{eff}

$$E_{\text{eff}} = \frac{\pi}{R}\sqrt{\frac{1}{6}}\left(\frac{k_1}{Q_1}\frac{A_{1,\text{free}}}{A_{1,\text{set}}}\cos\phi_1\right)^{-1/2}\left(\frac{2k_2\Delta f_2}{f_2}\right)^{3/2} \tag{2}$$

These equations assume the AFM tip can be described by a flat punch with radius R, which is used for all data presented in this work. Other geometries, such as sphere or cone, are derived elsewhere.[26] Other groups have preferentially used the sphere model for analyzing similar data.[27] In principle, the ability to choose a characteristic tip shape opens the door to an absolute modulus measurement—meaning that armed with well characterized tip shapes and dimensions these models have the potential to allow modulus measurements with no free parameters. In practice, AFM tip shapes are not commonly well characterized so we have taken a different approach of using a material with a "reference" modulus to characterize the tip size parameter (the tip radius R). This calibration procedure is explained below.

The key assumption in bimodal AFM theory is that the indentation depth δ is much smaller than the amplitude A_1. This is in fact achieved during AM-FM imaging in practice, where $\delta \approx 0.1-10$ nm, while typically $A_1 \approx 100$ nm. These are very small indentations depths relative to other mechanical testing techniques. The advantage of such small indentation depths is that the surface can be imaged with very high resolution and with minimal sample damage. The disadvantage of such low indentation depths is that the modulus measurement is more prone to errors and variations caused by surface effects such as roughness, adhesion, and contaminations.

Lastly, the tip−sample interaction stiffness k_{ts} presented throughout this work is calculated by

$$\langle k_{ts}\rangle = 2RE_{\text{eff}} = \pi\sqrt{\frac{2}{3}}\left(\frac{k_1}{Q_1}\frac{A_{1,\text{free}}}{A_{1,\text{set}}}\cos\phi_1\right)^{-1/2}\left(\frac{2k_2\Delta f_2}{f_2}\right)^{3/2} \tag{3}$$

where E_{eff} is calculated as described above for eqs 1 and 2.

Calibration. Calibration of the cantilever parameters k_1, k_2, f_1, f_2, Q_1, A_1 and the tip parameter R in eqs 1 and 2 is required for quantitative analysis of AM-FM data. A procedure for calibrating the stiffness of the cantilever's first resonant eigenmode as well as higher eigenmodes has been outlined in detail in recent work.[28] The approach involves measurements of the cantilever thermal noise and use of the equipartition theorem. This procedure also allows calibration of the cantilever deflection sensitivity (units nm/V) of both resonant eigenmodes, from which the cantilever oscillation amplitudes in nanometers can be determined. The thermal noise measurement also provides a measurement of the frequency and quality factor of both resonances.

An important parameter to determine accurately is the tip size, which here is defined by the punch model tip radius R. The simplest calibration approach is to perform an AM-FM measurement on a surface of known modulus prior to the

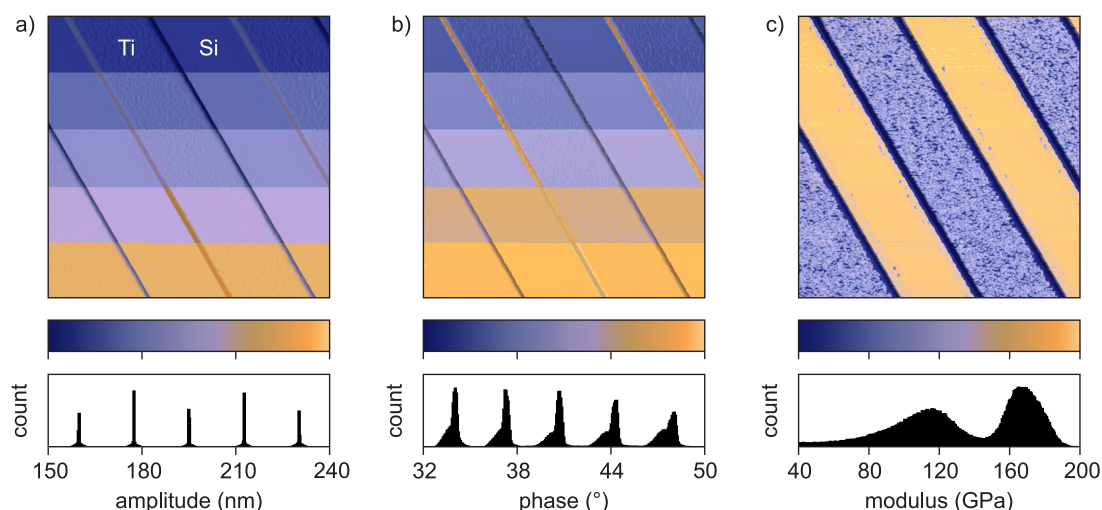indentation depth, which is required by bimodal AFM theory.[26,27]

Figure 4. AM-FM results for a Si sample with thin-film stripes of Ti. (a) The amplitude set point channel for the first eigenmode was increased incrementally from 160 to 230 nm (free air amplitude $A_{1,free}$ = 320 nm). (b) Phase image for the first eigenmode shows the resulting step increases corresponding to increases in the amplitude set point. (c) Elastic modulus image demonstrates the measured modulus is independent of amplitude set point. The indentation depths were 1.7 nm on Si and 1.9 nm on Ti. Cantilever: Olympus AC160 with $k_1 \approx 26$ N/m, $f_1 \approx 300$ kHz, $k_2 \approx 475$ N/m, and $f_2 \approx 1.7$ MHz. Scan size 10 μm.

experiment and extract the tip radius value that satisfies eq 2. Any difference between the modulus of this calibration or reference material and that of the sample leads to an increase in dependence on the choice of the assumed contact model (punch, sphere, or cone) used to analyze the AM-FM data. Therefore, it is advisable to minimize the difference in modulus between the reference material and the sample to reduce this model dependence.

As mentioned above, AFM cantilever tips often have ill-defined shapes and sizes. One common method that avoids explicitly characterizing this shape and size is the internal reference method. In this method, an area of the sample with known modulus (typically assumed as the accepted bulk value) is used to calibrate the tip radius. The resulting value of R is then applied to other areas of the sample or even different samples to obtain a modulus map. When using this internal reference method, errors in the other calibration parameters discussed above can be compensated by choosing a tip size scale that imposes the condition the measured modulus matches the reference modulus.

Quantitative Modulus Measurements. The ability of bimodal AM-FM imaging to accurately quantify nanoscale modulus can be demonstrated in the context of component identification in a multilayered packaging film. The film was known *a priori* to be composed of four polymers: polyethylene (PE), polypropylene (PP), polyethylene terephthalate (PET) and ethylene vinyl alcohol (EVOH). Calibration of both cantilever resonance spring constants was performed using a procedure outlined elsewhere,[28] while the calibration of the tip size was performed on a polystyrene reference sample, where the modulus was assumed to be 3.0 GPa.

Figure 2a shows the modulus map obtained by AM-FM imaging for this sample. By comparing the image to literature values of elastic moduli, the polymer constituents in each region were unambiguously identified by their relative values. The distinction between polymers is clear despite the small relative differences in modulus between the different film components and the indentation depths (<2 nm) shown in Figure 2b. For example, the PP and PET moduli differ by only

20%, yet they can be clearly distinguished in the AM-FM modulus map. The modulus distribution of each component, shown in the histogram in Figure 2c, is consistent with variations in the contact area that are likely linked to the sample roughness.

Wide Dynamic Range of Modulus Mapping. In addition to high sensitivity resolution of different materials with similar moduli as shown above, AM-FM imaging can be used to characterize materials across an extremely wide range of modulus. This is demonstrated in Figures 3a−e, which contain AM-FM modulus maps for samples spanning 3 orders of magnitude in modulus (∼0.1 to ∼200 GPa). The samples include polydimethylsiloxane (PDMS), thin films of polystyrene/polycaprolactone (PS/PCL) and polystyrene/polypropylene (PS/PP) polymer blends, lead/tin (Sn/Pb) solder alloy, and a patterned titanium (Ti) thin film on silicon (Si). (See Experimental Methods section for details on sample preparation.) Figure 3f summarizes these modulus maps in a single, logarithmic-scale histogram and provides information about the distribution in modulus for sample components.

Remarkably, all the modulus maps in Figure 3a−e were acquired using the same type of cantilever, shown in the inset in Figure 3f. In contrast, most nanomechanical testing techniques require the sensor's spring constant to be roughly matched to the tip−sample stiffness. The high sensitivity of AM-FM can be explained by the fact that changes in the effective cantilever stiffness due to tip−sample interactions are encoded as a frequency shift, which can be very reliably and accurately measured with a lockin amplifier.

A notable example of both the sensitivity and range of this technique is shown in Figure 3d where a 50:50 Sn/Pb alloy solder shows a pattern of softer and stiffer regions in the modulus channel that is not visible in topography (topography not shown; see ref 6). Often observed in optical and scanning electron micrographs,[29] this pattern is typical of Sn/Pb solder and is associated with softer, Pb-rich and stiffer, Sn-rich regions of solder. These regions were not identifiable with conventional AM imaging mode with a single resonance: they are not correlated with topographical or phase features; in addition,
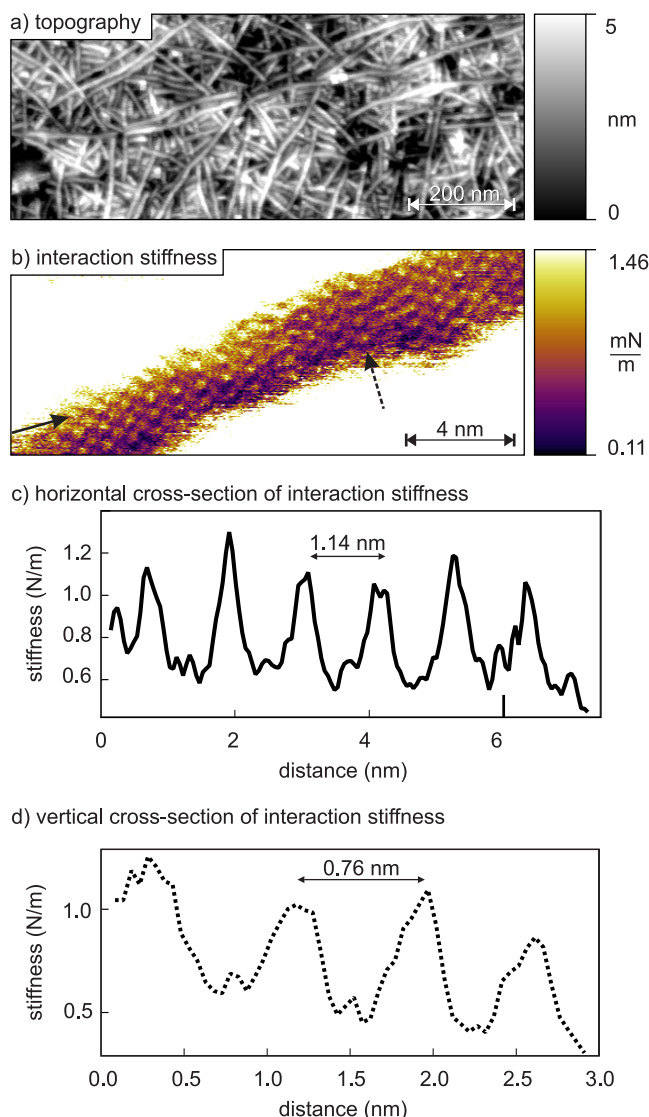
a) topography

b) interaction stiffness

c) horizontal cross-section of interaction stiffness

d) vertical cross-section of interaction stiffness

Figure 5. High spatial resolution imaging of syndiotactic polypropylene (sPP) in AM-FM mode. (a) Topography image of randomly distributed sPP crystallites. (b) Stiffness image of a single crystallite, where individual methyl groups of the polymer backbone are visible. (c) Line section along the crystallite in (b) in the direction of the solid arrow. The spacing between polymer chains is 1.14 ± 0.06 nm. (d) Line section along the polymer chain indicated by the dashed arrow in (b). The spacing between regular features is 0.76 ± 0.05 nm. Cantilever: NanoWorld ArrowUHF with $k_1 \approx 8.5$ N/m, $f_1 \approx 1.5$ MHz, $k_2 \approx 42$ N/m, and $f_2 \approx 4.5$ MHz.

loss tangent imaging was unable to distinguish them within measurement error.[6] Since the loss tangent is the ratio of the loss and storage moduli E″/E′, this lack of contrast may simply be due to these ratios being similar in the two materials or more likely, that the other artifacts as discussed in ref 6 overwhelm any differences in the material ratios. Since AM-FM imaging is sensitive to the storage modulus alone, it is not subject to this limitation and differences in the moduli are clearly visualized, as discussed in ref 6 (see specifically Figure 3 in ref 6 and associated discussion).

Measurements on High-Modulus Materials. Subresonance force measurement techniques such as force−distance curves are often used for modulus measurements with AFM. However, they cannot provide reliable modulus information on

very stiff materials due to the relatively low stiffness of commercial AFM cantilevers and the associated shallow indentation depths. In fact, very few AFM modes can quantitatively characterize nanomechanical properties of materials with moduli greater than a few tens of gigapascals.

Contact resonance AFM techniques[30−32] provide the ability to characterize mechanical properties of very stiff samples. However, the downside to such contact mode techniques is that the high normal forces (typically >100 nN) required for imaging can be destructive. This is especially problematic for very high-aspect-ratio features common to the semiconductor industry.

In contrast, the tapping-mode nature of AM-FM bimodal imaging means the tip contacts the sample intermittently, allowing nondestructive imaging and the ability to characterize high modulus samples by virtue of the high stiffness of higher cantilever eigenmodes. An example is shown in Figure 4, where AM-FM modulus mapping was performed on a Si wafer with a regular pattern of ~200 nm-high diagonal Ti. Here, the Si surface was used as an internal reference with an assumed modulus of 165 GPa, which led to a measured Ti modulus of 115 GPa. This measurement is consistent with the bulk modulus of 110−125 GPa.[33]

In addition, Figure 4 demonstrates the independence of the measured modulus on the AM-FM amplitude set point as it was varied stepwise during image acquisition. This variation was performed to test the applicability of modulus calculations to the experimental results. Whereas these deliberate changes led to horizontal bands visible in the amplitude and phase images (Figure 4a and b), the calculated modulus map (Figure 4c) does not show any corresponding variations. This implies that both the chosen tip contact model and bimodal theory used to perform the calculation were accurate for this data set. In this case, the Hertz model with punch tip geometry and radius R = 3.3 nm was used.

Molecular-Level Spatial Resolution. In addition to quantitative measurements, AM-FM mode can be used for high resolution imaging. We demonstrate this ability by imaging the structure of semicrystalline polymers on a molecular level. Although similar resolution has been reported previously,[34,35] it relied on custom cantilevers with specialized, extra-sharp tips operating in a torsional tapping mode. In contrast, for AM-FM imaging shown here, we used standard, commercially available cantilevers and obtained similar or better resolution images. Of course, AM-FM imaging also provides quantitative stiffness information alongside the topographic mapping.

It is important to note that for such high-resolution imaging, the continuum mechanics contact models used elsewhere in this work do not apply, mostly because the sample cannot be considered a semi-infinite half plane. Interpretation of the data in terms of modulus requires additional considerations beyond the scope of this article. Therefore, results in this section are presented in terms of the $\langle k_{ts} \rangle$. (Specifically, the reported tip−sample interaction stiffness in this section is the time-averaged stiffness change of the second eigenmode of the cantilever during intermittent contact experience while AM-FM imaging, as described in detail in ref 26.)

In the first example, long (>500 nm) crystallites of syndiotactic polypropylene (sPP) formed during solvent evaporation while spin-coating were imaged in AM-FM mode. In the topography image shown in Figure 5a, the height difference between crystalline features is ~5 nm. Figure 5b
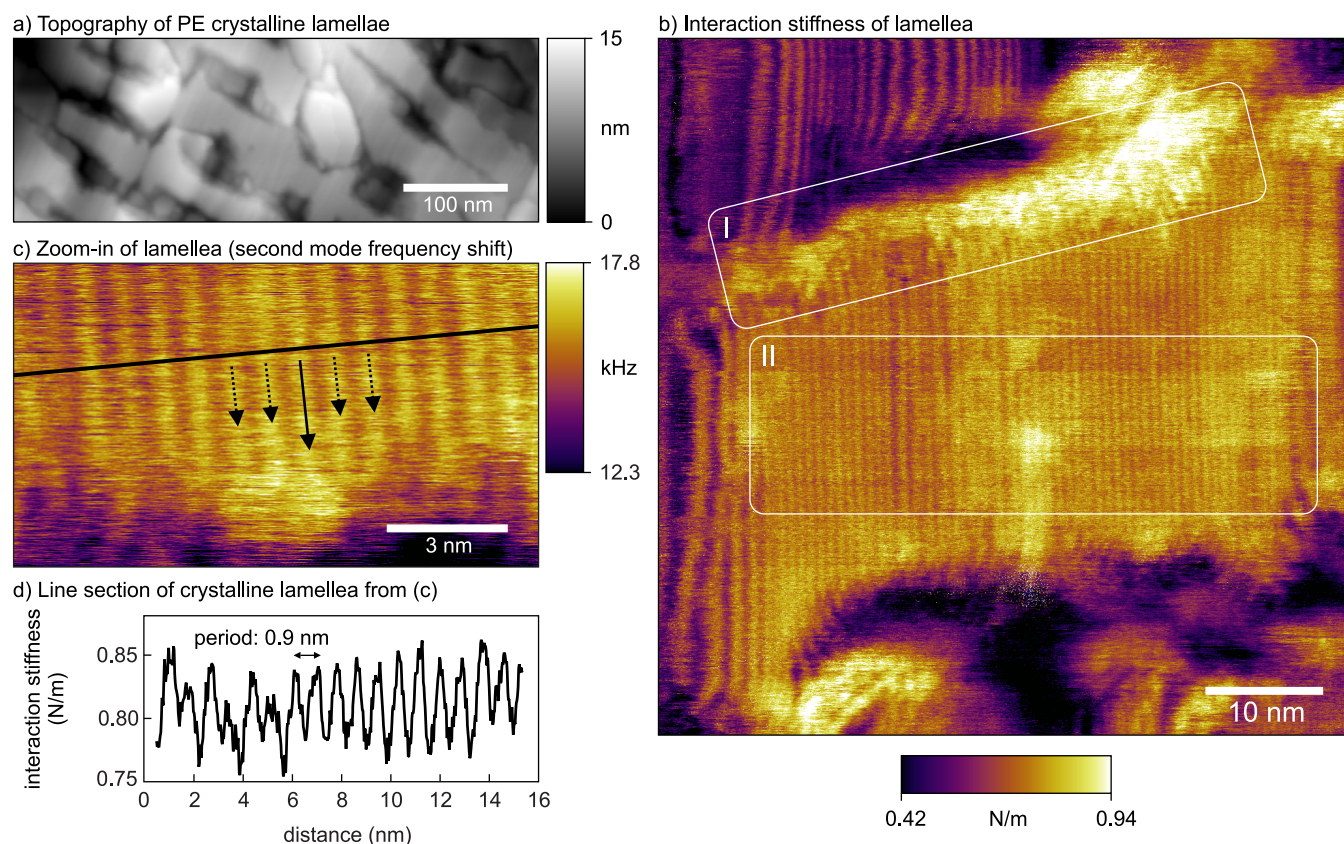
a) Topography of PE crystalline lamellae

b) Interaction stiffness of lamellea

c) Zoom-in of lamellea (second mode frequency shift)

d) Line section of crystalline lamellea from (c)

period: 0.9 nm

Figure 6. High spatial resolution imaging of polyethylene (PE). (a) Topography image of PE crystalline lamellae. (b) Tip−sample interaction stiffness image of a lamella with disordered end chains at the interface of the crystalline and amorphous phases (region I) and tightly packed polymer chains (region II). Blue pixels represent data points with NaN values, where negative indentation was calculated and was deemed unphysical. (c) Expanded image of tightly packed chains showing polymer chains looping out and back into the crystalline phase (solid arrows) and one of the polymer chains extending from crystalline into amorphous phase (dashed arrow). (d) Line section corresponding to the black line in (c) shows a 0.9 ± 0.1 nm spacing of polymer chains. See Figure S3 for additional PE sample features such as terrace steps. Cantilever: NanoWorld ArrowUHF with $k_1 \approx 8.5$ N/m, $f_1 \approx 1.5$ MHz, $k_2 \approx 42$ N/m, and $f_2 \approx 4.5$ MHz.

shows a tip−sample interaction stiffness map of a single crystallite, where the crystal lattice of the polymer is clearly visible. The distance between the regular features parallel to the crystallite (indicated by the solid arrow in Figure 5b) was measured to be 1.14 ± 0.06 nm, while the distance between regular features perpendicular to the crystallite (dashed arrow in Figure 5b) was 0.76 ± 0.05 nm. (Measurement uncertainty represents one standard deviation in the individual measurements.) Additionally, Fast Fourier Transforms (FFT) of the tip−sample interaction stiffness image confirms the periodicity of the observed features (see Supporting Information, Figure S1). These values correspond closely to the X-ray crystallography values of $b = 1.12$ nm and $c = 0.74$ nm predicted for the crystal lattice of sPP.[36]

In the second example, high spatial resolution AM-FM imaging was demonstrated on polyethylene (PE). In Figure 6a, the topography image displays flat lamellae distinctive of crystalline PE. The tip−sample interaction stiffness image with smaller scan size in Figure 6b highlights two regions: (I) the interface between crystalline and amorphous phases of the polymer and (II) tight packing of polymer chains within the crystalline region.

Figure 6c is a magnification of the interface region (region I in Figure 6b). Regularly aligned, tightly packed polymer chains are clearly visible. While most of the polymer chains loop out and back into the PE crystalline phase, some chains occasionally extend from the ordered crystalline phase into the disordered amorphous phase. This type of conformational arrangement of polymer chains has been predicted by theory and simulation[37] and is believed to be a factor in polymer crystallization that in turn affects bulk material properties. FFT of the tip−sample interaction stiffness image show a periodicity of 0.88 nm (see Figure S2). Measurements of line sections such as the one in Figure 6d yield 0.9 ± 0.1 nm for the spacing between the tightly packed chains, in good agreement with the value of 0.809 nm obtained by X-ray crystallography results for mechanically deformed PE samples.[38]

High-resolution AM-FM imaging can also be achieved in liquid environments, as demonstrated by the image of DNA in buffer solution in Figure 7. The double helix conformation of the DNA strands was resolved in the topographic and the interaction stiffness map of the AM-FM images. The 3.4 nm double helix pitch is clearly visible, with the major and minor groove widths of 2.2 and 1.2 nm, respectively, in the B conformation of the molecule. Ido *et al.*[39] have demonstrated very high resolution imaging of DNA topography in fluid, even beyond the helix resolution shown here. However, we have demonstrated quantitative characterization of the localized stiffness of the molecule, not only the topography. In addition, AM-FM imaging of biological materials has also been demonstrated in air.[40]
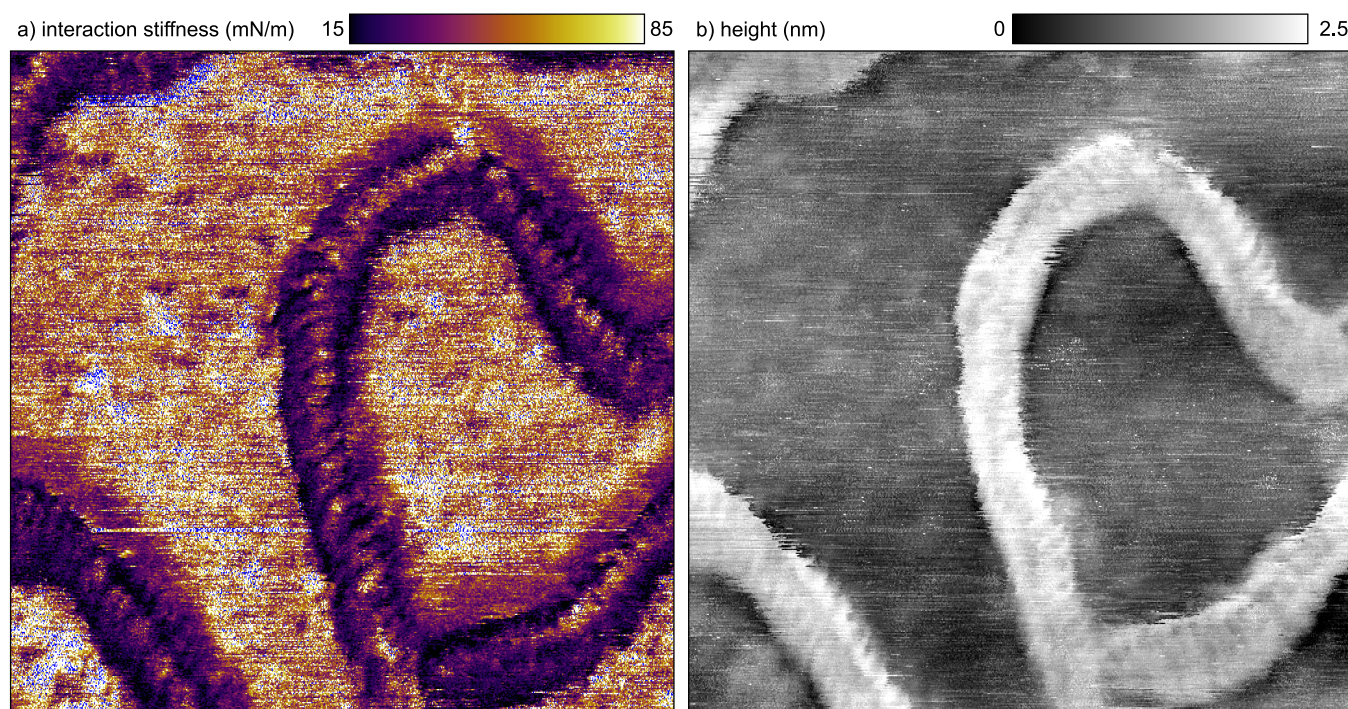
a) interaction stiffness (mN/m) 15 ... 85 b) height (nm) 0 ... 2.5

Figure 7. Molecular-resolution AM-FM interaction stiffness (k_{ts}) map and topography of DNA immobilized on mica in $NiCl_2$ buffer. The double helix of the DNA strand is resolved. Here, k_2 was calibrated by assuming the stiffness-frequency power law relationship of an Euler–Bernoulli beam.[28] Blue pixels represent data points with NaN values, where negative indentation was calculated and was deemed unphysical. Cantilever: Olympus AC40TS with $k_1 \approx 0.12$ N/m, $f_1 \approx 31$ kHz, $k_2 \approx 10.0$ N/m, and $f_2 \approx 283$ kHz. Scan size 72 nm.

Fast Nanomechanical Mapping. Small cantilevers with resonant frequencies in the megahertz can be used to perform AM-FM imaging at very rapid scan rates while preserving nanomechanical information and spatial resolution. This imaging is much faster than other nanomechanical techniques such as force curve mapping, contact resonance AFM, and fast force curve mapping based on pulsed force AFM.[41,42]

Fast AM-FM imaging is demonstrated in Figure 8, which shows a PS/PP polymer film imaged at increasing line scan rates. As the line scan rate increased from 2 to 39 Hz, the corresponding acquisition time for a complete 256 × 256 pixel image decreased from 128 to 6.5 s. Despite the expected compromise between image quality and scanning speed, the modulus mapping remains relatively accurate even at very high speeds. Analysis of the histogram in Figure 8g indicates the measured modulus of PP is observed to increase by less than 10% for a 20× increase in scanning speed. We expect that imaging rates will increase as faster cantilevers and microscopes become available.

CONCLUSIONS

Tapping mode is arguably the most successful and popular AFM imaging technique. Yet despite 30 years of use and development, quantitative, repeatable, and accurate estimation of sample moduli from tapping mode imaging has not made it into the mainstream. This work demonstrates that the addition of extra observables from bimodal operation of the cantilever during imaging enables modulus mapping on a wide range of materials. Modulus mapping was performed with bimodal AM-FM techniques on samples ranging from compliant polymers with low modulus (∼0.1−3 GPa) to very stiff metals with high modulus (>100 GPa). Notably, the results show that the same cantilever can quantitatively image modulus across 3 orders of

magnitude, provided the cantilever tip size is calibrated on an appropriate reference sample. Furthermore, molecular-level spatial resolution was achieved with AM-FM imaging on polymer chains in ambient conditions and revealed chain spacing and conformation predicted by theory and other experimental methods. Lastly, the tapping-mode basis of AM-FM mode enables high imaging speeds: quantitative nanomechanical imaging was demonstrated at rates nearing 5 s per image with only slight degradation in modulus accuracy. With these capabilities for fast imaging, high-resolution nanomechanical mapping over a wide modulus range, AM-FM imaging is likely to prove a valuable nanoscale characterization tool for many applications.

EXPERIMENTAL METHODS

Instrument. All experiments were performed on Cypher S and Cypher-ES AFMs (Asylum Research—an Oxford Instruments Company, Santa Barbara, CA) equipped with blueDrive photothermal excitation. The cantilevers used for imaging were AC160 and AC40 (Olympus, Tokyo, Japan) and ArrowUHF (NanoWorld. Neuchâtel, Switzerland). All cantilevers had a reflective coating on the back side.

Sample Preparation. *1. Thin-Film Polymer Blends.* Thin-film polymer blend samples of polystyrene/polypropylene (PS/PP) and polystyrene/polycaprolactone (PS/PCL) were prepared in-house by spin coating (Model WS-400BZ-6NPP/LITE, Laurell Technologies Corp., North Wales, PA) polymer solutions onto silicon wafers (orientation ⟨100⟩, p-type/boron doped, Silicon Quest International, San Jose, CA). Polystyrene pellets (430102, Sigma-Aldrich, St. Louis, MO) and polypropylene pellets (452157, Sigma-Aldrich, St. Louis, MO) were dissolved in *p*-xylene (99%, Alfa Aesar, Ward Hill, MA) in 3:1 ratio. Polystyrene pellets and polycaprolactone pellets (440744, Sigma-Aldrich, St. Louis, MO) were dissolved in chloroform (Product #C2432, Sigma-Aldrich, St. Louis, MO) in 2:1 ratio. All the films were >30 nm in thickness.
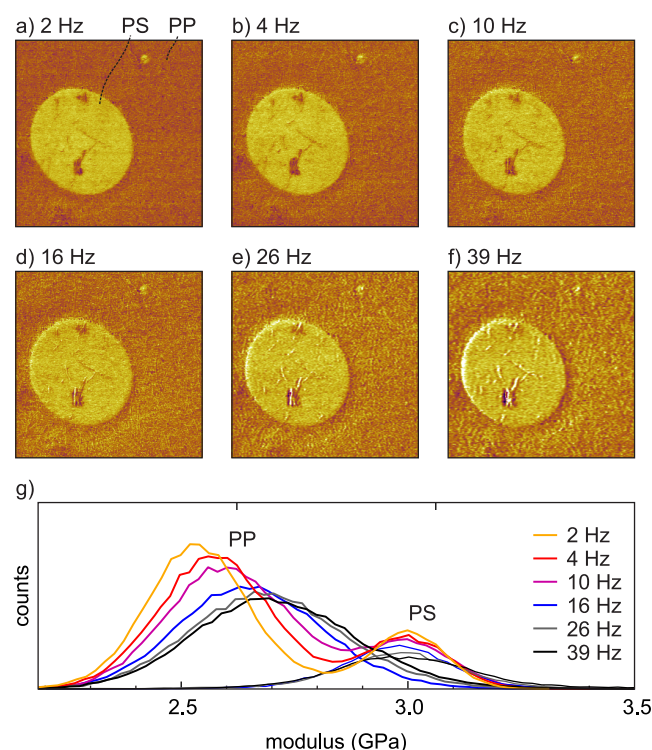
Figure 8. (a−f) Scan rate dependent AM-FM modulus images of a polystyrene/polypropylene (PS/PP) film obtained at increasing imaging speeds. The line scan rates of 2, 4, 10, 16, 26, and 39 Hz correspond to acquisition times of 128, 66, 26, 16.5, 9.8, and 6.5 s, respectively, for these 256 × 256 pixel images. (g) Histogram of all images demonstrates modulus changes with increasing imaging rates. A PS region of the sample was used as an internal reference with an assumed modulus of 3 GPa. This demonstrates the ability of the method to separate materials with very similar moduli at very rapid scan rates. Cantilever: NanoWorld ArrowUHF with $k_1 \approx 7$ N/m, $f_1 \approx 1.2$ MHz, $k_2 \approx 35$ N/m, and $f_2 \approx 3.5$ MHz. Scan size 2.5 μm. The small change in the measured polypropylene modulus is directly attributable to small changes in the observables associated with increased feedback errors as the scan rate increases.

2. Polyethylene (PE). The PE sample used for high-resolution imaging was prepared by the procedure published by Mullin and Hobbs.[35] A small amount of 82.9 kDa polyethylene (PSS-pe83k, Polymer Standards Service USA, Amherst, MA) was heated on a glass slide and then mechanically sheared as the sample cooled.

3. Polydimethylsiloxane (PDMS). The PDMS sample was prepared by molding silicone elastomer (Sylgard 184 encapsulant, Dow Corning, Auburn, MI) at 1:10 ratio and curing at 60 °C.

4. Multilayer Polymer Packaging Film. The multilayer polymer sample was prepared by placing the film in a clamp inside a cryomicrotome (EM UC7 cryochamber, Leica Microsystems, Buffalo Grove, IL) at −120 °C. Slices ~100 nm thick were removed from the sample until a cross section of the material was obtained. The sample was then thawed under a flow of nitrogen and imaged. Experiments involving a reference sample used a 2 × 2 mm² piece of ultrahigh-molecular-weight polyethylene[43] (UHMWPE) that had been cryomicrotomed at −80 °C.

5. Tin−Lead (Sn/Pb) Solder. The solder sample was prepared by melting ~0.5 g of a 50:50 Sn/Pb solder wire (Alpha Fry, Cookson Electronics Assembly Materials, South Plainfield, NJ), depositing it on freshly cleaved mica sheet, and heating the sample on a hot plate. Once the solder had melted, another mica sheet was used to press against the molten solder to obtain a flat sample. The mica was removed after the sample had cooled.

6. Silicon−Titanium (Si−Ti) Grid. A piece of Si wafer patterned with a ~200 nm thick Ti film[32] was cleaned by consecutive sonication in

acetone (HPLC grade, Alfa Aesar, Ward Hill, MA), isopropanol (Gigabit, KMG Chemicals Inc., Houston, TX), and ultrapure water (18.2 MΩ). The sample was dried with dry nitrogen and exposed to oxygen plasma for 1 min (PE-IIA, Technics).

7. DNA. A stock solution of Lambda DNA BstE II Digest (D-9793,Sigma-Aldrich, St. Louis, MO) stored at 4 °C in Tris-EDTA buffer at a concentration of 100 ng/μL was diluted to 10 ng/μL in a NiCl₂ buffer (10 mM NiCl₂, 40 mM Hepes, pH 6.8) immediately prior to use. 100 μL of this 10 ng/μL solution was applied on a freshly cleaved mica disc (diameter 1.5 cm). The mica disc had been previously attached to a metal puck using 24-h epoxy (04005, Harman, Belleville, NJ). The solution of DNA was incubated for 10 min and thoroughly rinsed using a 2 mL syringe filled with deionized water and a needle. This pressured water flush ensured attachment of DNA molecules on the surface. Finally, 150 μL of NiCl₂ buffer was added at the surface of the mica, and the preparation was then placed inside the AFM to be imaged.

ASSOCIATED CONTENT

⑤ Supporting Information

The Supporting Information is available free of charge on the ACS Publications website at DOI: 10.1021/acsnano.7b04530.

AFM images and FFTs (PDF)

AUTHOR INFORMATION

Corresponding Author

*E-mail: roger.proksch@oxinst.com.

ORCID ⓘ

Roger Proksch: 0000-0003-2124-1201

Notes

The authors declare the following competing financial interest(s): We are employed by a company that manufactures atomic force microscopes that use some of the techniques described in the manuscript.

REFERENCES

(1) Garcia, R. *Amplitude Modulation Atomic Force Microscopy*; Wiley, 2010.

(2) Herruzo, E. T.; Perrino, A. P.; Garcia, R. Fast Nanomechanical Spectroscopy of Soft Matter. *Nat. Commun.* **2014**, *5*, 3126.

(3) Proksch, R.; Yablon, D. G. Loss Tangent Imaging: Theory and Simulations of Repulsive-Mode Tapping Atomic Force Microscopy. *Appl. Phys. Lett.* **2012**, *100*, 073106.

(4) Cleveland, J. P.; Anczykowski, B.; Schmid, A. E.; Elings, V. B. Energy Dissipation in Tapping-Mode Atomic Force Microscopy. *Appl. Phys. Lett.* **1998**, *72*, 2613−2615.

(5) Paulo, Á. S.; García, R. Unifying Theory of Tapping-Mode Atomic-Force Microscopy. *Phys. Rev. B: Condens. Matter Mater. Phys.* **2002**, *66*, 41406.

(6) Proksch, R.; Kocun, M.; Hurley, D.; Viani, M.; Labuda, A.; Meinhold, W.; Bemis, J. Practical Loss Tangent Imaging with Amplitude-Modulated Atomic Force Microscopy. *J. Appl. Phys.* **2016**, *119*, 134901.

(7) Rodrıiguez, T. R.; Garcia, R. Compositional Mapping of Surfaces in Atomic Force Microscopy by Excitation of the Second Normal Mode of the Microcantilever. *Appl. Phys. Lett.* **2004**, *84*, 449.

(8) Proksch, R. Multifrequency, Repulsive-Mode Amplitude-Modulated Atomic Force Microscopy. *Appl. Phys. Lett.* **2006**, *89*, 113121.

(9) Lai, C.-Y.; Santos, S.; Chiesa, M. Systematic Multidimensional Quantification of Nanoscale Systems From Bimodal Atomic Force Microscopy Data. *ACS Nano* **2016**, *10*, 6265−6272.

(10) Santos, S.; Lai, C.-Y.; Olukan, T.; Chiesa, M. Multifrequency AFM: From Origins to Convergence. *Nanoscale* **2017**, *9*, 5038−5043.

(11) Garcia, R.; Herruzo, E. T. The Emergence of Multifrequency Force Microscopy. *Nat. Nanotechnol.* **2012**, *7*, 217−226.

(12) Zhong, Q.; Inniss, D.; Kjoller, K.; Elings, V. B. Fractured Polymer/silica Fiber Surface Studied by Tapping Mode Atomic Force Microscopy. *Surf. Sci.* **1993**, *290*, L688−L692.

(13) Hölscher, H. Quantitative Measurement of Tip-Sample Interactions in Amplitude Modulation Atomic Force Microscopy. *Appl. Phys. Lett.* **2006**, *89*, 123109.

(14) Lee, M.; Jhe, W. General Theory of Amplitude-Modulation Atomic Force Microscopy. *Phys. Rev. Lett.* **2006**, *97*, 36104.

(15) Hu, S.; Raman, A. Inverting Amplitude and Phase to Reconstruct Tip−sample Interaction Forces in Tapping Mode Atomic Force Microscopy. *Nanotechnology* **2008**, *19*, 375704.

(16) Katan, A. J.; van Es, M. H.; Oosterkamp, T. H. Quantitative Force *versus* Distance Measurements in Amplitude Modulation AFM: A Novel Force Inversion Technique. *Nanotechnology* **2009**, *20*, 165703.

(17) Fukuma, T.; Kilpatrick, J. I.; Jarvis, S. P. Phase Modulation Atomic Force Microscope with True Atomic Resolution. *Rev. Sci. Instrum.* **2006**, *77*, 123703.

(18) Sugawara, Y.; Kobayashi, N.; Kawakami, M.; Li, Y. J.; Naitoh, Y.; Kageshima, M. Elimination of Instabilities in Phase Shift Curves in Phase-Modulation Atomic Force Microscopy in Constant-Amplitude Mode. *Appl. Phys. Lett.* **2007**, *90*, 194104.

(19) Hölscher, H. Theory of Phase-Modulation Atomic Force Microscopy with Constant-Oscillation Amplitude. *J. Appl. Phys.* **2008**, *103*, 64317.

(20) Labuda, A.; Kobayashi, K.; Kiracofe, D.; Suzuki, K.; Grütter, P. H.; Yamada, H. Comparison of Photothermal and Piezoacoustic Excitation Methods for Frequency and Phase Modulation Atomic Force Microscopy in Liquid Environments. *AIP Adv.* **2011**, *1*, 22136.

(21) Albrecht, T. R.; Grütter, P.; Horne, D.; Rugar, D. Frequency Modulation Detection Using High-Q Cantilevers for Enhanced Force Microscope Sensitivity. *J. Appl. Phys.* **1991**, *69*, 668.

(22) Sader, J. E.; Jarvis, S. P. Accurate Formulas for Interaction Force and Energy in Frequency Modulation Force Spectroscopy. *Appl. Phys. Lett.* **2004**, *84*, 1801.

(23) Labuda, A.; Miyahara, Y.; Cockins, L.; Grütter, P. H. Decoupling Conservative and Dissipative Forces in Frequency Modulation Atomic Force Microscopy. *Phys. Rev. B: Condens. Matter Mater. Phys.* **2011**, *84*, 125433.

(24) Garcia, R.; Proksch, R. Nanomechanical Mapping of Soft Matter by Bimodal Force Microscopy. *Eur. Polym. J.* **2013**, *49*, 1897−1906.

(25) Amo, C. A.; Perrino, A. P.; Payam, A. F.; Garcia, R. Mapping Elastic Properties of Heterogeneous Materials in Liquid with Angstrom-Scale Resolution. *ACS Nano* **2017**, *11*, 8650.

(26) Labuda, A.; Kocuń, M.; Meinhold, W.; Walters, D.; Proksch, R. Generalized Hertz Model for Bimodal Nanomechanical Mapping. *Beilstein J. Nanotechnol.* **2016**, *7*, 970−982.

(27) Herruzo, E. T.; Garcia, R. Theoretical Study of the Frequency Shift in Bimodal FM-AFM by Fractional Calculus. *Beilstein J. Nanotechnol.* **2012**, *3*, 198−206.

(28) Labuda, A.; Kocun, M.; Lysy, M.; Walsh, T.; Meinhold, J.; Proksch, T.; Meinhold, W.; Anderson, C.; Proksch, R. Calibration of Higher Eigenmodes of Cantilevers. *Rev. Sci. Instrum.* **2016**, *87*, 73705.

(29) Basaran, C.; Jiang, J. Measuring Intrinsic Elastic Modulus of Pb/Sn Solder Alloys. *Mech. Mater.* **2002**, *34*, 349.

(30) Rabe, U. Atomic Force Acoustic Microscopy. In *Applied Scanning Probe Methods II: Scanning Probe Microscopy Techniques*; Bhushan, B., Fuchs, H., Eds.; Springer: Berlin, 2006; pp 37−90.

(31) Kocun, M.; Labuda, A.; Gannepalli, A.; Proksch, R. Contact Resonance Atomic Force Microscopy Imaging in Air and Water Using Photothermal Excitation. *Rev. Sci. Instrum.* **2015**, *86*, 83706.

(32) Tu, Q.; Lange, B.; Parlak, Z.; Lopes, J. M. J.; Blum, V.; Zauscher, S. Quantitative Subsurface Atomic Structure Fingerprint for 2D Materials and Heterostructures by First-Principles-Calibrated Contact-Resonance Atomic Force Microscopy. *ACS Nano* **2016**, *10*, 6491−6500.

(33) *Materials Properties Handbook Titanium Alloys*; Boyer, R., Welsch, G., Collings, E. W., Eds.; ASM International: Materials Park, 1994.

(34) Mullin, N.; Hobbs, J. K. Direct Imaging of Polyethylene Films at Single-Chain Resolution with Torsional Tapping Atomic Force Microscopy. *Phys. Rev. Lett.* **2011**, *107*, 197801.

(35) Savage, R. C.; Mullin, N.; Hobbs, J. K. Molecular Conformation at the Crystal−Amorphous Interface in Polyethylene. *Macromolecules* **2015**, *48*, 6160−6165.

(36) Lovinger, A. J.; Lotz, B.; Davis, D. D.; Padden, F. J. Structure and Defects in Fully Syndiotactic Polypropylene. *Macromolecules* **1993**, *26*, 3494−3503.

(37) Balijepalli, S.; Rutledge, G. C. Conformational Statistics of Polymer Chains in the Interphase of Semi-Crystalline Polymers. *Comput. Theor. Polym. Sci.* **2000**, *10*, 103−113.

(38) Seto, T.; Hara, T.; Tanaka, K.; Frank, F. C.; Tanaka, K.; Slichter, W. P.; Holmes, P. W. T.; Turner-Jones, A.; Kiho, H.; Hayashida, T. Phase Transformation and Deformation Processes in Oriented Polyethylene. *Jpn. J. Appl. Phys.* **1968**, *7*, 31−42.

(39) Ido, S.; Kimura, K.; Oyabu, N.; Kobayashi, K.; Tsukada, M.; Matsushige, K.; Yamada, H. Beyond the Helix Pitch: Direct Visualization of Native DNA in Aqueous Solution. *ACS Nano* **2013**, *7*, 1817−1822.

(40) Lamour, G.; Yip, C. K.; Li, H.; Gsponer, J. High Intrinsic Mechanical Flexibility of Mouse Prion Nanofibrils Revealed by Measurements of Axial and Radial Young's Moduli. *ACS Nano* **2014**, *8*, 3851−3861.

(41) Krotil, H.-U.; Stifter, T.; Waschipky, H.; Weishaupt, K.; Hild, S.; Marti, O. Pulsed Force Mode: A New Method for the Investigation of Surface Properties. *Surf. Interface Anal.* **1999**, *27*, 336−340.

(42) Amo, C. A.; Garcia, R. Fundamental High-Speed Limits in Single-Molecule, Single-Cell, and Nanoscale Force Spectroscopies. *ACS Nano* **2016**, *10*, 7117−7124.

(43) NIST Reference Material (RM) 8456.